

# Identification of cryptic neoepitopes generated by chimeric transcripts in ovarian cancer

**Vaishnavi M Dixit**

National Centre For Cell Science

**Arpita K Wagle**

Savitribai Phule Pune University

**Sharmila Bapat** (✉ [sabapat@nccs.res.in](mailto:sabapat@nccs.res.in))

National Centre For Cell Science <https://orcid.org/0000-0002-9557-2233>

---

## Research Article

### Keywords:

**Posted Date:** May 19th, 2022

**DOI:** <https://doi.org/10.21203/rs.3.rs-1456664/v2>

**License:** © ⓘ This work is licensed under a Creative Commons Attribution 4.0 International License.

[Read Full License](#)

---

# Abstract

Peptides identified in a customized targeted database were assessed for antigenicity. Further docking of peptide – MHC as well as peptide-MHC-TCR complexes provided proof-of-concept of antigenicity. Considerable recent interest lies in the immunogenicity of non-canonical neoantigens generated by alternative ORFs emerging from non-synonymous mutations or nucleotide insertions and deletions, exonization of untranslated regions of the genome, non-coding transcripts, transposable elements, etc. Amongst these ‘cryptic’ epitopes, those derived from chimeric transcripts which harbor sequences derived from more than one gene remain undefined, since the translational potential and immunogenicity of these transcripts is relatively unexplored. The present study was hence designed to predict and assess the neoepitopes generated by chimeric transcripts in ovarian cancer. Using a customized targeted database, we identified peptides uniquely generated by such transcripts, expressed either as reading-frame or sense/anti-sense isoforms. Further assessment of the antigenicity of these peptides identified a small number of putative neoepitopes that are likely to be presented to MHC-I in an allele-specific manner, and further recognized by specific TCRs. Effectively, such generation of chimeric molecules by relaxed rigidity of canonical transcription and translation may present opportunities in immunotherapy.

## Introduction

The tractability of gene boundaries through gene and transcript fusions presents a wide horizon of transcript diversity, especially in aberrant cellular contexts such as cancer<sup>1–3</sup>. Chimeric transcripts (CTs) harboring sequences derived from more than one gene represents one such class of transcript diversity. The constancy of structural complexities of CTs across tumor types, arising from differential splicing and/or inclusion of regulatory, canonically untranslated sequences suggests a non-random mechanism of their origin<sup>4–5</sup>. While it is believed that a majority of such CTs are eliminated by cellular surveillance mechanisms including nonsense mediated decay, a few reportedly generate fusion proteins<sup>6–7</sup>.

Current interests in cancer vaccines rely on discovery of effective tumor-specific neoepitopes<sup>8–11</sup>, since they elicit T-cell responses that are not subject to host central tolerance, and also lower extent of autoimmune toxicities<sup>12–13</sup>. Conventionally, tumor-specific non-synonymous mutations ‘reorganize’ the ORFs of protein-coding genes and perturb canonical protein sequences to generate neoepitopes that may be recognized and bound by specific T-cell receptors<sup>14–16</sup>. Personalized neoantigen discovery and validation remains a challenge since current algorithms rely on the binding affinity of putative neoantigens to HLA-I, while immunopeptidomics is complexed by the need for motif deconvolution in multi-allelic datasets<sup>18–21</sup>. Several cancers associated with a low mutational burden including acute lymphoblastic leukemia, high-grade serous ovarian (HGSC), prostate and pancreatic cancer generate functional CD8<sup>+</sup> T cell responses suggesting the presence of neoantigens<sup>22–23</sup>. HGSC is considered as being immunologically ‘cold’ with a mutational landscape largely restricted to *TP53*, *BRCA1* and *BRCA2*<sup>24</sup>. Yet, a fraction of tumors presents with high tumor infiltrating lymphocytes, wherein a

dominance of CD8 + cells correlate with improved prognosis<sup>25</sup>. This suggests a possibility of neoantigens being generated through other mechanisms.

On this background we hypothesized that chimeric transcripts identified in the TCGA ovarian cancer RNA sequencing datasets may be translated to generate novel chimeric, tumor-specific peptides, and a few of these presented as neoepitopes to CD8 + cells. We tested this by initially detecting their translational products in mass spectrometry datasets using a customized targeted chimeric transcript derived peptide database for identification of chimeric peptides. These peptides were further assessed for potential antigenicity *via* prediction of proteasome/ immunoproteasome processing, ferrying of degradation products to the endoplasmic reticulum by the transporter associated with antigen processing (TAP), recognition, binding to major histocompatibility complex class I (MHC-I) molecules for presentation and recognition by specific CD8<sup>+</sup> T-cell receptors (TCRs) that would mark the tumor cell for destruction. Identification of such chimeric epitopes highlights the cross-talks between relaxed transcription, translation and host immunity, which could be harnessed towards immunotherapy.

## Material And Methods

### Identification of Chimeric Transcript Longest Read-derived peptides (cLRPs)

We identified several candidate chimeric transcripts (CTs) in TCGA RNA-Seq data from 160 OvCa samples applying a customized computational workflow on the Seven Bridges Cancer Genomics Cloud platform (SBgenomics; <http://www.cancer-genomics-cloud.org>). All spanning reads of each CT was consolidated to derive longest read (LR) CT sequences (ranged between 71–148 bp). To resolve the coding capabilities of CTs, we developed a customized chimeric LR peptide (cLRP) database comprising of *in silico* translation of all LR sequences in 6 reading frames (RF) along with ENSP protein sequences and randomly generated decoy peptides (<https://www.ensembl.org>). This was applied as a backend reference for probing ovarian tumor mass spectra datasets generated by the National Cancer Institute Clinical Proteomic Tumor Analysis Consortium (CPTAC; Edwards et al. 2015), using the Fenyolab x tandem pipeline on the SBGenomics Cloud (Fig.S1a). This pipeline uses the X! Tandem search engine with pre-defined search parameters (Ruggles et al.2016; Ardeljan et al. 2019). Peptide Spectral Matches (PSMs) that qualified a confidence threshold were selected from outputs of this X!Tandem-based pipeline. Corresponding iTRAQ reporter ion intensities from spectral data (3 tumor samples and 1 site-specific pooled reference (labeled either with iTRAQ 117@PNNL/114@JHU) were extracted for computation of relative peptide abundances from sample enrichment ratios and summation of reporter ion intensities from different scans and bRPLC fractions; selecting for FDR values < 0.01 (expect values  $10^{-02}$ ). Thence the order of magnitude of relative peptide expression range was computed as log<sub>2</sub> transformed total peptide abundance. Examination of the charge state of PSMs in terms of b- and y- ion fragmentation profiles was performed using Proteome Discoverer™ (Thermo Scientific™).

### Prediction of antigenicity

Predictions of 9–11 residue degradation products of the tumor-specific cLRPs using the PCPS Proteasomal Cleavage Prediction Server (<http://imed.med.ucm.es/Tools/pcps/>) were followed by deploying TAPPred server for predicting binding affinity of peptides (IC50) towards the TAP transporter (<http://crdd.osdd.net/raghava/tappred/>) and generating TAP Scores. MHC Class-I alleles were selected for screening from two geographical regions *viz.* India (South Asia) and US (North America) from the HLA Allele Frequency Net Database (<http://www.allelefreqencies.net>; A:B:C alleles – 245:404:120) as is outlined in detail in Supplementary Figs. 1). Binding of peptides to MHC Class I was predicted using Netmhspan 4.1 that implements Neural Network Aligning (N-N Align) and is trained on Binding Affinity (BA) Data and Eluted Ligand (EL) datasets from mass spectrometry to present antigen to MHC molecules using concurrent motif deconvolution (process of associating ligand to MHC molecule), and rank peptides based on BA as a percentile score with respect to predication of top 100 peptides; hence lower BA rank corresponds to strong MHC I binders. Haplotype-based determination of the stability and affinity of potential neoantigens was determined by NetMHCstabpan1.0 (NetMHCstabpan – 1.0 - Services - DTU Health Tech) that predicts stability and affinity of a peptide towards an allele; a threshold of 0.5% combined rank stability was set to identify peptides most likely to bind to MHC molecules with T-Half (Predicted Half Life) > 2h and IC50 values < 100nM. Derivation of Allele Harmonic Binding Rank (AHBR) and Peptide Harmonic Best Rank (PHBR) was performed as described in Supplementary Methods.

### **Peptide MHC Docking**

Peptide structures were designed in PepFold3D model 1 structure (by convention considered most stable) was visualized in PyMol 4.2 and torsion angles edited using AutoDock 4. PDB structures of relevant and available HLA molecules were downloaded from IMGT and cleared of peptide ligands and artifacts from X-Ray crystallographic analysis using PyMol 4.2. These were submitted to CASTp for prediction of six peptide binding pockets within each molecule as described in Supplementary Methods.

### **Gibbs Motif analysis**

Gibbs Cluster 2.0 [GibbsCluster-2.0 Server (dtu.dk)] was applied to input test peptide sequences along with a set of validated restricting peptides for respective alleles obtained from MHCBN (A comprehensive database of MHC binding and Non-binding peptides; osdd.net, VDJDdb (cdr3.net) and published literature (Cole et.al 2006). Default MHC class I parameters were selected to identify clusters with highest Kullback-Leiber distance and probability scores to predict a binding motif for each allele.

### **Determination of Agretopicity Index and Validation of antigenicity of parental proteins**

A modified agretopicity Index was derived to compare the binding affinities of antigenic epitopes with corresponding 8-11-mer amino acid sequences in the 6-frame *in silico* translated outputs of its transcript sequence. Shorter peptides generated in some cases due to the presence of stop codons in the alternative frames, were disregarded and only 9-mers were processed (NetMHCstabpan 1.0) for comparison of affinities with the same allele. Similarly, 6-frame protein isoforms of the specific parental transcripts generating the cLR of PSEN2-CABC1 transcript, *viz.* PSEN2-001 (ENST00000366783.3) and

CABC1,ADCK3-004 (ENST00000366779.1; Ensembl Genome Browser, <https://www.ensembl.org>, Homo\_sapiens - GRCh37) were predicted *in silico*, and each of the 12 generated proteins were processed through established pipeline for prediction of antigenicity as above.

### **Docking of p:MHC:TCR complexes**

CDR3 sequences of  $\alpha$  and  $\beta$  chains with associated V and J genes of the available pMHC-TCR complexed with alleles HLA-A\*11:01, HLA-A\*24:02 and HLA-B\*27:05 (Ladell, 2014) were derived from VDJ database (VDJdb : <https://cdr3.net>). This provided references of 2 TCR:viral (EBV) epitopes:HLA-A\*11:01:2; 18 TCRs: human epitopes: HLA-A\*24:02:4; and 1 TCR:viral (HIV) epitopes:HLA-B\*27:05:4; (ImmuneScape VDJ Assembler, <https://tcr2.cs.biu.ac.il/home>; <https://sysimm.ifrec.osaka-u.ac.jp/immune-scape/mhc1>). 10 peptides restricting 3 alleles were modeled with respective complexed TCR, selecting TCR sequences where epitope of human origin was available; in case of epitopes of viral origin, TCR structures with minimum VDJdb acquisition Score of 1 were considered as structure of confidence. ERGOS II (<https://biu.ac.il>) was used to derive p:MHC:TCR binding scores for test peptide:allele complex and CDR3 sequences of  $\alpha$  and  $\beta$  chain sequences with associated V and J genes. Autoencoder-based model along with VDJ Database as training set were provided as parameters. ImmuneScape VDJ chain assembler derived full length chain sequences of TCR- $\alpha\beta$  using CDR3 and VJ genes were further provided for modeling in ImmuneScape Modeler along with epitope and HLA-Alleles to obtain PDB output, which in turn was provided as input to TCR 3D repertoire database (<https://umd.edu>) for derivation of Incident and docking angles and TCR-CoM coordinates. Further, PyMol and Discovery Studio were used to visualize PDB structures for comparison of polar bond lengths and interacting residues with reference PDB structures obtained in VDJdb wherever available. while another complex structure was generated for HLA-A\*11:01 towards evaluation of obtained TCR-p:MHC complexes.

### **Comparison with pre-reported neoantigens**

Pre-validated neoantigens reported in Melanoma (Ott et.al,2020) and Glioblastoma (Keskin et.al, 2019) were processed through the same pipeline deployed in the present study. For the melanoma dataset, a reference peptide, DELEIKAY reported to restrict HLA-B\*18:01 (PDB ID:4XXC <https://www.rcsb.org/structure/4XXC>) was selected for simulation of docking and comparison of interactions with predicted peptides. 2 TCRs, *viz.* TRAV19\*01-J3\*01: TRBV20-1\*01-J2-7\*01; TRAV1-2\*01-J32\*01:TRBV18\*01-J1-4\*01 reported to complex with HLA-B\*18:01 and epitopes of human origin (EEAAGIGIL, MEVDPIGHLY; VDJ assembler) were derived to execute the second level of molecular modeling was and identify similar interactions as those in respective references. For glioblastoma, simulation of docking was performed and compared with reported reference, RRKWRRWHL for peptides predicted to restrict HLA-B\*27:05 (<https://www.rcsb.org/structure/5IB1>) and further for secondary docking with TCR TRAV14/DV4/J21-TRBV6-5\*01/J1-1\*01 reportedly complexed with HLA-B\*27:05 and epitopes of Viral HIV origin (KRWILGLNK; VDJ assembler) for comparison of interactions as those of reference.

### **Statistical Analysis**

Two groups of patients were demarcated within the cohort based on their TcTP burden (lower and higher than median values of CTs and cLRPs), *viz.* Group 1 (n = 51, low TcTP) and Group 2 (n = 50, high TcTP). Kaplan Meier (K-M) plots were constructed using survival package in R and tested for significance by log-rank test ( $p < 0.05$ ). Differences between the K-M curves for the 2 groups were computed using survival probability as function of time and by inspecting the visual shape of plots, median overall survival (OS) and progression-free survival (PFS) in days. Between and within group analysis of variance (ANOVA) was performed for derived AHBR and PHBR values to segregate the variation of peptide distribution and allele restriction for two groups. Trends in distribution across G1 and G2 were analyzed through one-way ANOVA (Kruskal-Wallis H-test, performed using Microsoft Excel 2019 Office Analysis ToolPak), testing null hypothesis stating equal mean values of both groups which was rejected if calculated value (F-value) was observed to be greater than the critical chi-square value (F-crit) at  $p < 0.05$ . Additional attributes (number of predicted antigenic peptides through NetMHCpan, number of these peptides detected in mass spectra, summation of relative abundance of cLRPs and MS detected antigenic peptides, allele restriction by NetMHCpan predicted antigenic peptides and mass spectrometry detected antigenic peptides, total AHBR-PHBR score, patient OS in days) were extracted and scaled based on their minimum to maximum values for visualization in MeV (Multiple Experiment Viewer v4.9).

## Results

### *Translation of chimeric transcripts (CTs) in ovarian cancer generates tumor-specific (TS) peptides*

A necessary first step was to identify peptides generated from chimeric transcript (CT) sequences around the fusionpoint identified in the TCGA ovarian cancer RNA-sequencing datasets. We consolidated all spanning reads of each CT to derive long read (LR) sequences for focused analyses rather than full-length transcript sequences since our working hypothesis was to evaluate chimeric peptides harboring residues of both parental proteins which were likely to be tumor-specific and perceived as non-self by the cellular machinery. Thus, 997 unique chimeric LR-derived peptides (cLRPs) were identified in ovarian tumor mass spectra datasets generated by the National Cancer Institute Clinical Proteomic Tumor Analysis Consortium<sup>26</sup> (CPTAC) using a X! Tandem search engine-based pipeline and a targeted chimeric LR-derived peptide (cLRP) database<sup>27-28</sup> (Fig.S1a; Methods) on the Seven Bridges Cancer Genomics Cloud<sup>29</sup>. Each tumor displayed a distinct profile of 28–132 cLRPs with a relative peptide expression range between 3.5-8 orders of magnitude (Fig. 1a-i). Since false-positive rates for PSM subgroups can vary (different peptide sizes, charge state of precursor ions, missed enzymatic cleavage, etc.), we affirmed chimerism by examining the charge state of PSMs in terms of b- and y- ion fragmentation profiles (Fig.S1b). While most peptides were transcribed from a single reading-frame (RF) without preferential usage of sense / antisense strands, RF isoforms of the same CT were also identified in some cases (Figs.S1c,S1d).

Tumor and tissue specificity was further inferred by probing expression of cLRPs in ovarian controls (OvCtrls; CPTAC data analyzed in parallel with tumor data), and human lymphoblastoid cell line data<sup>30</sup> (LBL; PXD001406). OvCtrls and LBLs displayed distinct cLRP profiles at frequencies of 29–49 and 0–9

/sample respectively, with corresponding relative peptide expression between 3.5–6.7 and 2-4.08 orders of magnitude. cLRP frequency as well as expression levels were lower in OvCtrls over primary tumors and even lower in LBL cultures (Figs. 1a-i,a-ii,a-iii). Peptide profiling designated 843 cLRPs to be Ovarian Tumor-Specific (TS), while remaining were Tumor-Associated (TA). Effectively, translation potential could be assigned to only 21.12% of the identified CTs as affirmed by the specificity imposed by ion fragmentation profiling. Such lower coding capability as compared to that of parental genes despite the enhanced peptide diversity *via* RF isoforms of a single CT may indicate either a non-coding regulatory nature of CTs, or elimination of newly formed proteins by cell surveillance and homeostatic mechanisms.

Tumor associated Chimeric Transcript-Protein (TcTP) burden may define MHC-I allele restriction by cLRPs and patient prognosis in a personalized manner

While oncogenic roles have been recently assigned to CTs<sup>31</sup>, it is likely that several chimeric proteins may fail to achieve a stable conformation and thereby targeted for proteasomal degradation. Interestingly, recent findings suggest cryptic neoepitopes generated through proteasomal degradation bind to MHC class I molecules and are presented to CD8+ cells in eliciting anti-tumor responses<sup>32–35</sup>. To evaluate a similar possible fate within the 844 tumor-specific cLRPs in our study, we first predicted their constitutive and immunoproteasome degradation products using the Proteasomal Cleavage Prediction Server followed by identifying good and moderate strong binding peptides to the transporter associated with antigen processing protein complex (TAP; binding scores 6–7, 7–8 and 8-9.5 respectively) on TAPPred server (Methods). Further presentation of these 526 9-mer peptides to MHC Class I molecules was screened using NetMHCPan 4.1 in a set of 769 high frequency restricted MHC Class-I alleles representing Indian and Caucasian populations derived from the HLA Allele Frequency Net Database<sup>36</sup> (Supplementary Information 1). This identified 369 peptides that restrict 98.9% of selected MHC alleles with a Binding Affinity (BA) Rank  $\leq 0.5\%$ ; restriction being either between single or multiple peptide-alleles (Fig.S2; Tables S1, S2, S3). We also determined the Patient Harmonic Mean Best Rank (PHBR) and Allele Harmonic Binding Rank (AHBR) scores for these 369 putatively antigenic peptides, and correlated them with cLRP frequencies and relative expression in patients along with non-antigenic cLRP-derived peptides (Figs. 1b; Methods). This winnowed out a subset of 248 peptides (PHBR and AHBR  $< 0.3$ ), whose wider distribution across patients and higher binding rank within the restricted HLA alleles indicated higher probability of their antigenicity (Fig. 1c; Table S4).

We further examined the association of CTs and cLRPs in terms of a tumor-associated Chimeric Transcript-Protein (TcTP) burden, with overall patient survival (OS) in the cohort. This identified 2 distinct groups; patients in Cluster1 with lower average OS presented with a lower TcTP burden ( $< 60$  CTs,  $< 40$  cLRPs), while Cluster 2 patients with significantly higher average OS presented with higher TcTP burden ( $> 65$  CTs,  $> 55$  cLRPs; Fig. 2a). As a corollary, differences in outcomes between patient groups in the TCGA cohort demarcated on the basis of median CT-cLRP values in the cohort as either Group 1 (lower TcTP burden) or Group 2 (higher TcTP burden) also indicated a chimerism-based survival advantage (Fig. 2b). Importantly, the variance between PHBR and AHBR within both groups was significant while only AHBR between the 2 groups was significant (Fig. 2c), emphasizing possible improved presentation

and specificity in binding of cLRP to MHC-I alleles. Consolidation of all such parameters accentuated differences between the 2 groups of patients demarcated based on their TcTP burden (Fig. 2d-I). Lower TcTP (Group1) tumors were associated with fewer antigenic peptides and of a lower relative abundance, hence are likely to restrict fewer MHC-I alleles than Group 2 tumors with higher TcTP (Figs. 2d-II to 2d-VI). Most importantly, cLRP derived neoantigens as a determinant of patient allele(s) are suggested to influence prognosis; this allele-specificity of cLRPs could serve as protective factor in a personalized manner and effectively impart a survival advantage in at least a subset of ovarian cancer patients (Fig. 2d-VII). Overall, a certain threshold of TcTP burden may be essential to assign a CT-derived survival advantage, especially on the background of rare outliers in Group 1 that could imply other, unknown protective mechanisms.

Positional amino acid binding preferences in cLRP-derived epitope-MHC complexes exhibit homology with binding pocket preferences of reference peptide:MHC structures

We increased the stringency of our prediction pipeline through haplotype-based determination of the stability and affinity of these potential neoantigens (NetMHCstabpan1.0; Methods), to identify a subset of 55 peptides restricting 117 HLA alleles at a high confidence and significant BA rank (p:MHC interactions;  $\text{Thalf} > 2$ ;  $\text{IC50} < 100\text{nm}$ ; Table S5; Figs. 3a,3b; Fig.S3). HLA-C alleles were strikingly absent in this subset that represent cLRP derivatives most likely to harbor neoantigenic potential, including a highly stability ASCSVAWSW:HLA-B\*57:26 complex ( $\text{Thalf} = 31.44\text{h}$ ), while ATIRTVSSW:HLA-B\*58:19 presented with highest affinity ( $\text{IC50} = 3.12\text{nM}$ ). Figure 3

Further molecular modelling of the p:MHC interactions was performed using reported PDB allele structures (<http://www.IMGT/3Dstructure-DB>). 12 MHC allele structures were thus available within our list of restricted alleles, which interact with 27 peptides in 39 complexes, 27 of which display significant polar, electrostatic, and hydrophobic interactions (Figs.S4a,S4b). Within these, we performed Gibbs motif analyses for 7 complexes (for which binding pocket details were available in elucidated crystal p:MHC structures; Methods). This guided the assignment of positional residue specificity within cLR-p:MHC molecule interactions (Fig. 3c). Further comparisons *vis-à-vis* polar, electrostatic and hydrophobic interactions within these 7 complexes with reference to reference structures (RP:MHC) available for each allele revealed some identical interactions, amongst others involving interactions between a different peptide residue and the same MHC residue at a specific position (we termed these as MHC interactive residues; Table S6, Supplementary Information 4 Video 1 ).

Thus, the high probability positional residues identified through Gibbs Cluster analysis anchor ATQGRSWRK in HLA-A\*11:01 through interactions of A1 with T171 and E63 (pocket A, identical to reference), and K9 with Y99 (pocket D, MHC interactive residue); this complex is additionally stabilized through binding of T2 and Q3 with MHC interactive residues in pockets B and C respectively (Fig. 3d-i). Our observation of the KRMLASFSF:HLA-B\*27:09 complex being stabilized through 3 polar and 1 electrostatic bonds between R2 and B pocket residues (E45,E63,T24, identical to reference) is supported by an earlier report indicating pocket B of HLA-B\*27:09 to be sterically and electrostatically suited to bind

to arginine<sup>37</sup>. This complex displays additional bonds between K1 and MHC interactive residues in pocket A that create an outward directed kink in the peptide and exposes remaining residues (Fig. 3d-ii). A high probability positional Y9 residue anchors RQRQKRIAY in pocket F of HLA B\*15:01 identical to the reference, along with additional bonds between R1 and MHC interactive residues in pockets A and B (Fig. 3d-iii). Pocket B of HLA-B\*58:01 interacts with several residues of KQLLHSWKW including the high probability positional residues W9, S6 and K8; a predicted Y3-R97 salt bridge however may have a destabilizing effect (Fig. 3d-iv). The LAARPGPRW:HLA B\*57:03 and IFWDIFCRF:HLA-A\*24:02 models however did not compare favourably either with Gibbs analyses or comparative outputs with reference complexes (Figs.S4c-i,c-ii). The high probability positional R2 of RRTERAPRF:HLA-B\*27:05 displayed interactions with MHC interactive residues in pockets E and F, with additional stabilization through interactions of Y3,P7 and F9 with MHC interactive residues (Fig.S4c-iii). Conclusively, commonalities identified between cLRP- and R- p:MHC structures *vis-à-vis* involvement and positional preferences of specific residues of peptides and MHC molecules, will contribute to their recognition as neoepitopes.

### ***Antigenic epitopes present a low Agretopicity Index over corresponding sequence reading-frame / strand isoforms***

We assessed the agretopicity index of each of the 7 predicted p:MHC complexes to compare the affinities of antigenic epitopes with their alternative (8–11)-mer reading-frame/strand isoforms (Methods). All isoforms of the remaining peptides displayed lower affinity than the 7 test peptides (IC<sub>50</sub> > 800-fold higher; Fig.S5a; Table S7), indicating the latter to be more robust binders to the respective alleles. We further extended this theme by evaluating the 6 reading-frame protein isoforms of full-length parental protein isoforms for antigenicity, as is exemplified in PSEN2-CABC1 that harbors the peptide ATQGRSWRK (Figs.S5b;5c;5d). This identified 6 peptides restricting HLA-A\*11:01 (1 from PSEN2 and 5 from CABC1), all of which are derived from reading-frame / strand isoforms and none from the canonical parental proteins (Table S8). While all harbored the highest positional specificity binding residue K9 (predicted in Gibbs Motif analysis for HLA-A\*11:01), none of these peptides except ATQGRSWRK were detected in mass spectrometry, suggesting that a single RF of this cLRP was translated. This also revealed ATQGRSWRK as not being a chimeric peptide, but derived from a frame-shift in PSEN2 transcript.

### ***cLR-p:MHC:TCR complex stabilization involves dynamic interactions similar to reference structures***

A next level of molecular modeling to examine interactions involved in recognition of cLR-p:MHC complexes by  $\alpha$  and  $\beta$  chains of TCR was performed, which is the defining prelude to MHC-I mediated T-cell cytotoxicity. cLR-p:MHC:TCR complexes were generated considering the reported complementary CDR3 chain sequences available for 3 alleles (HLA-A\*24:02:4, HLA-A\*11:01:2, HLA-B\*27:05:4). Comparison of these models with reference epitope interactions displayed relatively similar ERGO II scores across all complexes, with those for ATQGRSWRK:HLA-A\*11:01 and KIINPIIRK:HLA-A\*11:01 being indicated at a higher confidence (Fig.S6a; Table S9). Interactions of ATQGRSWRK:HLA-A\*11:01 with 2 reported TCRs were examined and compared for stability and affinity with those of the 2 reference peptides (one each for MHC and TCR binding) *viz.* AIMPARFYPK:HLA-A\*11:01<sup>38</sup> (RP:MHC) and HLA-

A\*11:01-TCR: IVTDFSVIK<sup>39</sup> (RP-TCR). ATQGRSWRK:HLA-A\*11:01:TRAV21\*01/J50\*01-TRBV6.6\*01/J2.3\*01 complex displayed a strong binding score with 4 polar interactions similar to those in the RP:TCR (R5-S98; peptide:TCR- $\beta$  Figs. 4a-i,4a-ii) and RP:MHC (A1-Y7, A1-Y159 in A pocket; T2-E63 in B pocket; Fig. 4a-iii), which were further stabilized with *de novo* interactions including K9-D116 (MHC-F pocket; Fig. 4a-iv; Table S10). Alignment of crossing and incident angles ( $61.368^\circ$  and  $11.3246^\circ$  respectively) with a smaller  $\theta$  (x-axis angle of projection of the TCR:CoM–MHC:CoM vector;  $-33.41^\circ$ ) led to a diagonal placement of TCR on the cLR-p:MHC structure and facilitates a R5-S98 interaction (Fig. 4b, Fig. S6b, Supplementary Information 4 Video 2). Visualization of polar, hydrophobic and electrostatic clouds indicated evasion of steric hinderance; specifically, presentation of R5 towards the outside facing plane (surface) of the MHC groove along with a lateral shift of its amino terminal within the same pocket makes it available for interaction with the TCR- $\beta$  chain (Fig. S6c-i, 6c-ii, left panels). TCR recognition and R5-S98 interaction also achieves a robust anchoring of the peptide deeper into the hydrophobic MHC pocket (Fig. S6c-i, 6c-ii, right panels) enhancing stabilization of entire complex.

On the other hand, no interactions between peptide and TCR residues were evident in the ATQGRSWRK:HLA-A\*11:01: TRAV35\*01/J49\*01- TRBV11-2\*01/J1-2\*01 complex, although most of the polar, electrostatic and hydrophobic p:MHC interactions were retained and geometrical alignment of crossing and incident angles were similar to those within the ATQGRSWRK:HLA-A\*11:01:TRAV21\*01/J50\*01-TRBV6.6\*01/J2.3\*01 complex (Table 11; Fig. S6d). This is likely due to the steric hindrance generated by an altered TCR:CoM–MHC:CoM vector ( $\theta$ :  $-143.15^\circ$ ), which in turn results in a positional shift of S6 deeper into the MHC complex that collaterally decreases the possibility of R5 interacting with TCR- $\beta$ . Comparative modeling by superimposing ATQGRSWRK:HLA-A\*11:01 with the 2 reported TCRs further emphasized the planar shift and steric hinderance reducing the chances of p:TCR interactions within the A\*11:01: TRAV35\*01/J49\*01- TRBV11-2\*01/J1-2\*01 complex (Fig. 4c). Effectively, this highlights prioritization of neoepitopes through its recognition and binding to the TCR by, (i) determining the orientation and conformation of a firmly anchored peptide in the MHC molecule with specific exposed residues, and (ii) extent of perturbations within the p:MHC-I complex due to the proximity of a TCR through steric hinderance.

### ***Similar assessment of earlier reported immunizing mutated neoantigens affirms prediction analyses***

We further compared our evaluation with reported, tumor-specific mutated immunizing neoantigens in melanoma<sup>40</sup> and glioblastoma<sup>41</sup>. Processing of the reported immunizing mutated peptides in these studies through our stability- and affinity-based prediction identified 6 and 24 antigenic peptides in melanoma and glioblastoma respectively (Figs. 5a-i, 5b-i; Table S11; Figs. S7a; S7b; S7c). Molecular modeling of some of these, for example NEVSEVTVF-HLA-A\*18:01 (melanoma) revealed polar interactions (V8-R97; F9-W147) similar to those in reference p:MHC complex (Fig. 5a-ii; Table S12). Following TCR recognition and binding, the NEVSEVTEF:HLA-B\*18:01:TRAV1-2\*01-J32\*01:BV18\*01-J1-4\*01 complex displayed a polar p:MHC interaction (E2-S24) identical with the reference (DELEIKAY:HLA-B\*18:01), and unique p:TCR- $\alpha$  (polar:S4-G92) and p:TCR- $\beta$  (electrostatic:E8-K51; Fig. 5a-iii) interactions. A second complex NEVSEVTEF:HLA-B\*18:01:TRAV19\*01-J3\*01:BV20-1\*01-J2-7\*01 was characterized

with similar polar p:MHC interaction (E8-W147) and unique p:TCR- $\alpha$  (polar:S4-R96) and p:TCR- $\beta$  (electrostatic:E8-R99) interactions as compared with reference complexes.(Fig. 5b-iv).

The glioblastoma peptides AAHRARYFW and VSAHRARY restricting HLA-B\*27:05 display an overlap with the reported peptide ARYFWGNLA, which presents 3 polar p:MHC interactions (A2-E63, A2-R62, A2-Y159;Fig.S7d-i), and complexes with TRAV14/DV4/J21-TRBV6-5/J1-1 through three similar polar, and single electrostatic and hydrophobic p:MHC interactions (A1-Y171, A2-E63, A2-Y159, W9-D77, A1-W167 respectively) and exclusive polar (R4-P28, R6-N98) and hydrophobic (A5-Y52) interactions with TCR- $\alpha$  (Fig.S7d-ii,iii; Table S12). VSAHRARY displayed 6 similar polar p:MHC interactions (V1-Y171,V1-Y159,S2-E63,S2-R62,Y9-D77,Y9-W147) and a single hydrophobic interaction (V1-W167) as that of reported peptide, and interacts with TCR TRAV14/DV4/J21-TRBV6-5/J1-1 through five similar polar pMHC (V1-Y171,V1-Y7,V1-Y159,S2-E63,A3-Y99), and exclusive polar interactions in TCR- $\beta$  (A7-G98) and TCR- $\alpha$  (H5-Y52), and two exclusive electrostatic interactions TCR- $\alpha$  (R6-E95, R8-E30; Figs. 5b-ii;5b-iii;5b-iv). A few more peptides in both tumor datasets were indicated to be antigenic through Gibbs cluster motif analysis and docking (data not shown). Taken together, our prediction of neoepitopes generated from cLRPs represents a robust approach suggesting chimeric transcript derived proteins and their reading frame isoforms to present cryptic epitopes in tumors.

## Discussion

Genomic sequencing followed by evaluation of immunogenicity is a recognized neoantigen prediction approach towards personalized cancer therapy, especially in tumors with a high mutation burden<sup>42</sup>. An underlying assumption is that while most intragenic mutations would not alter gene expression and translation capabilities, they generate a tumor-specific protein modified, which could harbour a neoepitope capable of evoking host immunity. Chimeric transcripts on the other hand, being considered a fall-out of aberrant transcriptional and/or splicing machinery in a cell, often may not be translated and have not been evaluated as a source of neoantigens. The mass spectrometry-based identification of peptides derived from chimeric reads using a customized database was hence an essential prelude in our antigenicity prediction, and assigned protein-coding potential to around a fifth of the chimeras produced, a large majority of which were tumor-specific. While we began with the premise of screening only the chimeric peptides with residues of both partners, a realization was that chimera generation may also mediate frame-shift of either / both parental partners besides using of the anti-sense strand, to generate additional neoantigens. A further study towards derivation of full-length chimeric transcripts and mass-spectrometry based identification of their translation products to explore for neoantigenicity would widen the horizons of the present study.

Our assessment of the frequency of chimeric transcripts and peptides vis-a-vis a Chimeric Transcript-Protein (TcTP) burden indicated influences on overall patient survival in a personalized manner through MHC-I allele-specific restriction by some peptides. Modelling the latter at a molecular level revealed the complex dynamics of peptide recognition and presentation, which is challenging since a few thousand human MHC-I alleles are known, and individuals can express as many as six distinct alleles, each with

different epitope affinities. We hope that since our predictions were monoallelic, validation may widen the horizons of neoantigenicity to enhance the repertoire of peptide recognition. Allele – based patient stratification may thus identify individuals with an immune checkpoint blockade (ICB) benefit, as is reported in non-small-cell lung cancer and melanoma<sup>43</sup>. At the other end of the personalization spectrum, patients expressing HLA-I molecules with promiscuous peptide binding capabilities are indicated to display a significantly worse prognosis after ICB<sup>44</sup>. The specificity in recognition assigned through our modelling of the TCR interactions shifts the focus to peptide-TCR interactions as a definitive complementation to MHC-I based predictions and thereby strengthens the neoepitope prediction pipeline.

The field of chimeric neoepitopes is thus nascent as yet, and will require several further approaches as in case of other tumor-specific neoepitopes, to realize its full potential. Attrition of host responses through *in situ* systems influences of an immunosuppressive microenvironment (T-regs, cytokine balance, etc), inactivation of MHC-I and loss of antigen presentation, T-cell apoptosis/ exhaustion / anergy, altered immune checkpoints, etc. that define personalized features besides a patient's alleles will continue to present challenges<sup>45</sup>. Considered broadly, our findings including studying the conformation and dynamics of peptide-MHC-TCR interactions to qualify a *bona fide* neoepitope from chimeric transcript-derived peptides also contribute to understanding why only some of the several predicted neoantigens are likely to elicit immunogenicity; this will be useful in developing novel, immunogenicity based personalized therapies.

## Abbreviations

HGSC - High-grade serous ovarian tumors, ORF – Open Reading Frame, CTs - Chimeric transcripts, MHC-I - Major Histocompatibility Complex class I, TCR-T-cell receptor, TS-Tumor-Specific, LR- Long Read, cLRPs- Chimeric LR-derived Peptides, CPTAC- Clinical Proteomic Tumor Analysis Consortium, RF- Reading Frame, PSMs-Peptide Spectral Matches, OvCtrls- Ovarian Controls, LBL- Lymphoblastoid, TA- Tumor-Associated, AFND- Allele Frequency Net Database, BA Rank – Binding Affinity Rank, EL -Eluted Ligand, PHBR-Patient Harmonic Mean Best Rank, AHBR-Allele Harmonic Binding Rank, TOA- Tumor Ovarian control associated, TLA- Tumor-LBL associated, TcTP- Tumor-associated Chimeric Transcript-Protein, OS- Overall Survival, PFS- Progression Free Survival, pMHC- peptide MHC, RP:MHC- Reference Peptide MHC, cLR-p:MHC- Chimeric Longest Read peptide-MHC, cLR-p:MHC TCR- Chimeric Longest Read peptide-MHC TCR, RP-TCR Reference Peptide-TCR, TCR:CoM– TCR Centre of Mass, MHC:CoM- MHC Centre of Mass, PCPS- Proteasomal Cleavage Prediction Server, VDJdb -VDJ database, KM-Kaplan Meier, ANOVA- Analysis of Variance

## Declarations

### Author Contributions

SAB conceptualized and planned the study design, performed and curated proteomics analysis, VMD performed, analysed and interpreted experimental data and wrote the manuscript draft AW analysed

proteomics data using Proteome Discoverer™ and generated b-y ion plots. SAB supervised and interpreted experimental data and edited the manuscript draft to its final form.

## **Funding**

This work was supported by the Tata Innovation Fellowship of the Department of Biotechnology, Government of India (BT/HRD/35/01/04/2017), Fulbright-Nehru grants of USIEF (Award No. 2055/F-NAPE/2015), ICMR-DHR International Fellowship for Senior Bio-medical Scientists (INDO/FRC/452(S-60y2019-20-IHD). VMD was granted project research fellowship by Department of Biotechnology, (India BT/HRD/35/01/04/2017).

## **Availability of data and materials**

The materials that support the conclusion of this review have been included within the article.

## **Acknowledgements**

Research was supported by the Tata Innovation Fellowship of the department of Biotechnology, Government of India (BT/HRD/35/01/04/2017), Fulbright-Nehru grants of USIEF (Award No. 2055/F-NAPE/2015), ICMR-DHR International Fellowship for Senior Bio-medical Scientists (INDO/FRC/452(S-60;2019-20-IHD). VMD was granted project research fellowship by Department of Biotechnology, (India BT/HRD/35/01/04/2017). Data used in this publication were generated by the Clinical Proteomic Tumor Analysis Consortium (NCI/NIH) and is acknowledged. We extend our gratitude to Prof. David Fenyö and Dr. McKerrow, for sharing and explaining workflows of the FenyöLab xtandem pipeline on the SBGenomics Cloud. The collaborative grant with Seven Bridges Genomics (\$10,000 of compute and storage credits is deeply appreciated). The Seven Bridges Cancer Research Data Commons Cloud Resource has been funded in whole or in part with Federal funds from the National Cancer Institute, National Institutes of Health, Contract No. HHSN261201400008C and ID/IQ Agreement No. 17X146 under Contract No. HHSN261201500003I and 75N91019D00024 Technical assistance from Mr. Avinash Mali and support from the NCCS Proteomics facility are gratefully acknowledged. All figures in this manuscript were created using BioRender.com

## **Conflicts of Interest**

The authors declare no competing interests.

## **References**

1. Magnuson B, Bedi K, Ljungman M (2016) Genome stability versus transcript diversity. *DNA Repair* 44:81–86. <https://doi.org/10.1016/j.dnarep.2016.05.010>
2. Parris TZ (2020) Pan-cancer analyses of human nuclear receptors reveal transcriptome diversity and prognostic value across cancer types. *Sci Rep* 10(1):1873. <https://doi.org/10.1038/s41598-020-58842-6>

3. Cheng S, Li Z, Gao R, Xing B, Gao Y, Yang Y, Qin S, Zhang L, Ouyang H, Du P, Jiang L, Zhang B, Yang Y, Wang X, Ren X, Bei JX, Hu X, Bu Z, Ji J, Zhang Z (2021) A pan-cancer single-cell transcriptional atlas of tumor infiltrating myeloid cells. *Cell* 184(3):792–809e23. <https://doi.org/10.1016/j.cell.2021.01.010>
4. Gorohovski A, Tagore S, Palande V, Malka A, Raviv-Shay D, Frenkel-Morgenstern M (2017) ChiTaRS-3.1-the enhanced chimeric transcripts and RNA-seq database matched with protein-protein interactions. *Nucleic Acids Res* 45(D1):D790–D795. <https://doi.org/10.1093/nar/gkw1127>
5. Mukherjee S, Detroja R, Balamurali D, Matveishina E, Medvedeva YA, Valencia A, Gorohovski A, Frenkel-Morgenstern M (2021) Computational analysis of sense-antisense chimeric transcripts reveals their potential regulatory features and the landscape of expression in human cells. *NAR genomics and bioinformatics* 3(3):lqab074. <https://doi.org/10.1093/nargab/lqab074>
6. Jividen K, Li H (2014) Chimeric RNAs generated by intergenic splicing in normal and cancer cells. *Genes Chromosomes Cancer* 53(12):963–971. <https://doi.org/10.1002/gcc.22207>
7. Urbanski LM, Leclair N, Anczuków O (2018) Alternative-splicing defects in cancer: Splicing regulators and their downstream targets, guiding the way to novel cancer therapeutics. *Wiley interdisciplinary reviews RNA* 9(4):e1476. <https://doi.org/10.1002/wrna.1476>
8. Cafri G, Gartner JJ, Zaks T, Hopson K, Levin N, Paria BC, Parkhurst MR, Yossef R, Lowery FJ, Jafferji MS, Prickett TD, Goff SL, McGowan CT, Seitter S, Shindorf ML, Parikh A, Chatani PD, Robbins PF, Rosenberg SA (2020) mRNA vaccine-induced neoantigen-specific T cell immunity in patients with gastrointestinal cancer. *J Clin Invest* 130(11):5976–5988. <https://doi.org/10.1172/JCI134915>
9. Brohl AS, Sindiri S, Wei JS, Milewski D, Chou HC, Song YK, Wen X, Kumar J, Reardon HV, Mudunuri US, Collins JR, Nagaraj S, Gangalapudi V, Tyagi M, Zhu YJ, Masih KE, Yohe ME, Shern JF, Qi Y, Guha U, Khan J (2021) Immuno-transcriptomic profiling of extracranial pediatric solid malignancies. *Cell Rep* 37(8):110047. <https://doi.org/10.1016/j.celrep.2021.110047>
10. Verdon DJ, Jenkins MR (2021) Identification and Targeting of Mutant Peptide Neoantigens in Cancer Immunotherapy. *Cancers* 13(16):4245. <https://doi.org/10.3390/cancers13164245>
11. Roesler AS, Anderson KS (2022) Beyond Sequencing: Prioritizing and Delivering Neoantigens for Cancer Vaccines. *Methods Mol Biol* 2410:649–670. [https://doi.org/10.1007/978-1-0716-1884-4\\_35](https://doi.org/10.1007/978-1-0716-1884-4_35)
12. McGranahan N, Furness AJ, Rosenthal R, Ramskov S, Lyngaa R, Saini SK, Jamal-Hanjani M, Wilson GA, Birkbak NJ, Hiley CT, Watkins TB, Shafi S, Murugaesu N, Mitter R, Akarca AU, Linares J, Marafioti T, Henry JY, Van Allen EM, Miao D, Swanton C (2016) Clonal neoantigens elicit T cell immunoreactivity and sensitivity to immune checkpoint blockade. *Sci (New York N Y)* 351(6280):1463–1469. <https://doi.org/10.1126/science.aaf1490>
13. Jhunjhunwala S, Hammer C, Delamarre L (2021) Antigen presentation in cancer: insights into tumour immunogenicity and immune evasion. *Nat Rev Cancer* 21(5):298–312. <https://doi.org/10.1038/s41568-021-00339-z>
14. Parkhurst M, Gros A, Pasetto A, Prickett T, Crystal JS, Robbins P, Rosenberg SA (2017) Isolation of T-Cell Receptors Specifically Reactive with Mutated Tumor-Associated Antigens from Tumor-Infiltrating

- Lymphocytes Based on CD137 Expression. *Clin cancer research: official J Am Association Cancer Res* 23(10):2491–2505. <https://doi.org/10.1158/1078-0432.CCR-16-2680>
15. Veatch JR, Lee SM, Fitzgibbon M, Chow IT, Jesernig B, Schmitt T, Kong YY, Kargl J, Houghton AM, Thompson JA, McIntosh M, Kwok WW, Riddell SR (2018) Tumor-infiltrating BRAFV600E-specific CD4 + T cells correlated with complete clinical response in melanoma. *J Clin Investig* 128(4):1563–1568. <https://doi.org/10.1172/JCI98689>
  16. Joglekar AV, Li G (2021) T cell antigen discovery. *Nat Methods* 18(8):873–880. <https://doi.org/10.1038/s41592-020-0867-z>
  17. Ghorani E, Rosenthal R, McGranahan N, Reading JL, Lynch M, Peggs KS, Swanton C, Quezada SA (2018) Differential binding affinity of mutated peptides for MHC class I is a predictor of survival in advanced lung cancer and melanoma. *Annals of oncology: official journal of the European Society for Medical Oncology* 29(1):271–279. <https://doi.org/10.1093/annonc/mdx687>
  18. Wilson EA, Anderson KS (2018) Lost in the crowd: identifying targetable MHC class I neoepitopes for cancer immunotherapy. *Expert Rev Proteomics* 15(12):1065–1077. <https://doi.org/10.1080/14789450.2018.1545578>
  19. Alvarez B, Barra C, Nielsen M, Andreatta M (2018) Computational Tools for the Identification and Interpretation of Sequence Motifs in Immunopeptidomes. *Proteomics* 18(12):e1700252. <https://doi.org/10.1002/pmic.201700252>
  20. Freudenmann LK, Marcu A, Stevanović S (2018) Mapping the tumour human leukocyte antigen (HLA) ligandome by mass spectrometry. *Immunology* 154(3):331–345. <https://doi.org/10.1111/imm.12936>
  21. Hilf N, Kuttruff-Coqui S, Frenzel K, Bukur V, Stevanović S, Gouttefangeas C, Platten M, Tabatabai G, Dutoit V, van der Burg SH, Straten T, Martínez-Ricarte P, Ponsati F, Okada B, Lassen H, Admon U, Ottensmeier A, Ulges CH, Kreiter A, von Deimling S, Wick A, W (2019) Actively personalized vaccination trial for newly diagnosed glioblastoma. *Nature* 565(7738):240–245. <https://doi.org/10.1038/s41586-018-0810-y>
  22. Zamora AE, Crawford JC, Allen EK, Guo XJ, Bakke J, Carter RA, Abdelsamed HA, Moustaki A, Li Y, Chang TC, Awad W, Dallas MH, Mullighan CG, Downing JR, Geiger TL, Chen T, Green DR, Youngblood BA, Zhang J, Thomas PG (2019) Pediatric patients with acute lymphoblastic leukemia generate abundant and functional neoantigen-specific CD8<sup>+</sup> T cell responses. *Sci Transl Med* 11(498):eaat8549. <https://doi.org/10.1126/scitranslmed.aat8549>
  23. Yang W, Lee KW, Srivastava RM, Kuo F, Krishna C, Chowell D, Makarov V, Hoen D, Dalin MG, Wexler L, Ghossein R, Katabi N, Nadeem Z, Cohen MA, Tian SK, Robine N, Arora K, Geiger H, Agius P, Bouvier N, Morris L (2019) Immunogenic neoantigens derived from gene fusions stimulate T cell responses. *Nat Med* 25(5):767–775. <https://doi.org/10.1038/s41591-019-0434-2>
  24. Cancer Genome Atlas Research Network (2011) Integrated genomic analyses of ovarian carcinoma. *Nature* 474(7353):609–615. <https://doi.org/10.1038/nature10166>

25. Shih IM, Wang Y, Wang TL (2021) The Origin of Ovarian Cancer Species and Precancerous Landscape. *Am J Pathol* 191(1):26–39. <https://doi.org/10.1016/j.ajpath.2020.09.006>
26. Edwards NJ, Oberti M, Thangudu RR, Cai S, McGarvey PB, Jacob S, Madhavan S, Ketchum KA (2015) The CPTAC Data Portal: A Resource for Cancer Proteomics Research. *J Proteome Res* 14(6):2707–2713. <https://doi.org/10.1021/pr501254j>
27. Ruggles KV, Tang Z, Wang X, Grover H, Askenazi M, Teubl J, Cao S, McLellan MD, Clauser KR, Tabb DL, Mertins P, Slebos R, Erdmann-Gilmore P, Li S, Gunawardena HP, Xie L, Liu T, Zhou JY, Sun S, Hoadley KA, Fenyő D (2016) An Analysis of the Sensitivity of Proteogenomic Mapping of Somatic Mutations and Novel Splicing Events in Cancer. *Mol Cell proteomics: MCP* 15(3):1060–1071. <https://doi.org/10.1074/mcp.M115.056226>
28. Ardeljan D, Wang X, Oghbaie M, Taylor MS, Husband D, Deshpande V, Steranka JP, Gorbounov M, Yang WR, Sie B, Larman HB, Jiang H, Molloy KR, Altukhov I, Li Z, McKerrow W, Fenyő D, Burns KH, LaCava J (2019) LINE-1 ORF2p expression is nearly imperceptible in human cancers. *Mob DNA* 11:1. <https://doi.org/10.1186/s13100-019-0191-2>
29. Lau, J. W., Lehnert, E., Sethi, A., Malhotra, R., Kaushik, G., Onder, Z., Groves-Kirkby, N., Mihajlovic, A., DiGiovanna, J., Srdic, M., Bajcic, D., Radenkovic, J., Mladenovic, V., Krstanovic, D., Arsenijevic, V., Klisic, D., Mitrovic, M., Bogicevic, I., Kural, D., Davis-Dusenbery, B., ... Seven Bridges CGC Team (2017). The Cancer Genomics Cloud: Collaborative, Reproducible, and Democratized—A New Paradigm in Large-Scale Computational Research. *Cancer research*, 77(21), e3–e6. <https://doi.org/10.1158/0008-5472.CAN-17-0387>
30. Battle A, Khan Z, Wang SH, Mitrano A, Ford MJ, Pritchard JK, Gilad Y (2015) Genomic variation. Impact of regulatory variation from RNA to protein. *Sci (New York N Y)* 347(6222):664–667. <https://doi.org/10.1126/science.1260793>
31. Shi X, Singh S, Lin E, Li H (2021) Chimeric RNAs in cancer. *Adv Clin Chem* 100:1–35. <https://doi.org/10.1016/bs.acc.2020.04.001>
32. Karandikar SH, Sidney J, Sette A, Selby MJ, Korman AJ, Srivastava PK (2019) New epitopes in ovalbumin provide insights for cancer neoepitopes. *JCI insight* 5(8):e127882. <https://doi.org/10.1172/jci.insight.127882>
33. Erhard F, Dölken L, Schilling B, Schlosser A (2020) Identification of the Cryptic HLA-I Immunopeptidome. *Cancer Immunol Res* 8(8):1018–1026. <https://doi.org/10.1158/2326-6066.CIR-19-0886>
34. Roudko V, Bozkus CC, Orfanelli T, McClain CB, Carr C, O'Donnell T, Chakraborty L, Samstein R, Huang KL, Blank SV, Greenbaum B, Bhardwaj N (2020) Shared Immunogenic Poly-Epitope Frameshift Mutations in Microsatellite Unstable Tumors. *Cell* 183(6):1634–1649e17. <https://doi.org/10.1016/j.cell.2020.11.004>
35. Javitt A, Shmueli MD, Kramer MP, Kolodziejczyk AA, Cohen IJ, Kamer I, Litchfield K, Bab-Dinitz E, Zadok O, Neiens V, Ulman A, Radomir L, Wolf-Levy H, Eisenberg-Lerner A, Kacem A, Alon M, Rêgo AT,

- Stacher-Priehse E, Lindner M, Koch I, Bar J, Swanton C, Samuels Y, Levin Y, da Fonseca PCA, Elinav E, Friedman N, Meiners S, Merbl Y (2021)  
10.24.464690  
; doi: <https://doi.org/10.1101/2021.10.24.464690>
36. Gonzalez-Galarza FF, McCabe A, Santos E, Jones J, Takeshita L, Ortega-Rivera ND, Cid-Pavon G, Ramsbottom K, Ghattaoraya G, Alfirevic A, Middleton D, Jones AR (2020) Allele frequency net database (AFND) 2020 update: gold-standard data classification, open access genotype data and new query tools. *Nucleic Acids Res* 48(D1):D783–D788. <https://doi.org/10.1093/nar/gkz1029>
37. Hillig RC, Hülsmeier M, Saenger W, Welfle K, Misselwitz R, Welfle H, Kozerski C, Volz A, Uchanska-Ziegler B, Ziegler A (2004) Thermodynamic and structural analysis of peptide- and allele-dependent properties of two HLA-B27 subtypes exhibiting differential disease association. *J Biol Chem* 279(1):652–663. <https://doi.org/10.1074/jbc.M307457200>
38. Blicher T, Kastrup JS, Pedersen L, Buus S, Gajhede M (2006) Structure of HLA-A\*1101 in complex with a hepatitis B peptide homologue. *Acta Crystallogr Sect F Struct Biol Cryst Commun* 62(Pt 12):1179–1184. <https://doi.org/10.1107/S1744309106044228>
39. Zhang QJ, Gavioli R, Klein G, Masucci MG (1993) An HLA-A11-specific motif in nonamer peptides derived from viral and cellular proteins. *Proc Natl Acad Sci USA* 90(6):2217–2221. <https://doi.org/10.1073/pnas.90.6.2217>
40. Ott, P. A., Hu, Z., Keskin, D. B., Shukla, S. A., Sun, J., Bozym, D. J., Zhang, W., Luoma, A., Giobbie-Hurder, A., Peter, L., Chen, C., Olive, O., Carter, T. A., Li, S., Lieb, D. J., Eisenhaure, T., Gjini, E., Stevens, J., Lane, W. J., Javeri, I., ... Wu, C. J. (2017). An immunogenic personal neoantigen vaccine for patients with melanoma. *Nature*, 547(7662), 217–221. <https://doi.org/10.1038/nature22991>
41. Keskin, D. B., Anandappa, A. J., Sun, J., Tirosh, I., Mathewson, N. D., Li, S., Oliveira, G., Giobbie-Hurder, A., Felt, K., Gjini, E., Shukla, S. A., Hu, Z., Li, L., Le, P.M., Allesøe, R. L., Richman, A. R., Kowalczyk, M. S., Abdelrahman, S., Geduldig, J.E., Charbonneau, S., ... Reardon, D. A. (2019). Neoantigen vaccine generates intratumoral T cell responses in phase Ib glioblastoma trial. *Nature*, 565(7738), 234–239. <https://doi.org/10.1038/s41586-018-0792-9>
42. Hu, Z., Leet, D. E., Allesøe, R. L., Oliveira, G., Li, S., Luoma, A. M., Liu, J., Forman, J., Huang, T., Iorgulescu, J. B., Holden, R., Sarkizova, S., Gohil, S. H., Redd, R. A., Sun, J., Elagina, L., Giobbie-Hurder, A., Zhang, W., Peter, L., Ciantra, Z., ... Ott, P. A. (2021). Personal neoantigen vaccines induce persistent memory T cell responses and epitope spreading in patients with melanoma. *Nature medicine*, 27(3), 515–525. <https://doi.org/10.1038/s41591-020-01206-4>
43. Cummings, A. L., Gukasyan, J., Lu, H. Y., Grogan, T., Sunga, G., Fares, C. M., Hornstein, N., Zaretsky, J., Carroll, J., Bachrach, B., Akingbemi, W. O., Li, D., Noor, Z., Lisberg, A., Goldman, J. W., Elashoff, D., Bui, A., Ribas, A., Dubinett, S. M., Rossetti, M., ... Garon, E. B. (2020). Mutational landscape influences immunotherapy outcomes among patients with non-small-cell lung cancer with human leukocyte antigen supertype B44. *Nature cancer*, 1(12), 1167–1175. <https://doi.org/10.1038/s43018-020-00140-1>

44. Manczinger M, Koncz B, Balogh GM, Papp BT, Asztalos L, Kemény L, Papp B, Pál C (2021) Negative trade-off between neoantigen repertoire breadth and the specificity of HLA-I molecules shapes antitumor immunity. *Nat cancer* 2(9):950–961. <https://doi.org/10.1038/s43018-021-00226-4>
45. Oliveira, G., Stromhaug, K., Klaeger, S., Kula, T., Frederick, D. T., Le, P. M., Forman, J., Huang, T., Li, S., Zhang, W., Xu, Q., Cieri, N., Clauser, K. R., Shukla, S. A., Neuberger, D., Justesen, S., MacBeath, G., Carr, S. A., Fritsch, E. F., Hacohen, N.,... Wu, C. J. (2021). Phenotype, specificity and avidity of antitumour CD8<sup>+</sup> T cells in melanoma. *Nature*, 596(7870), 119–125. <https://doi.org/10.1038/s41586-021-03704-y>

## Figures

Fig.1

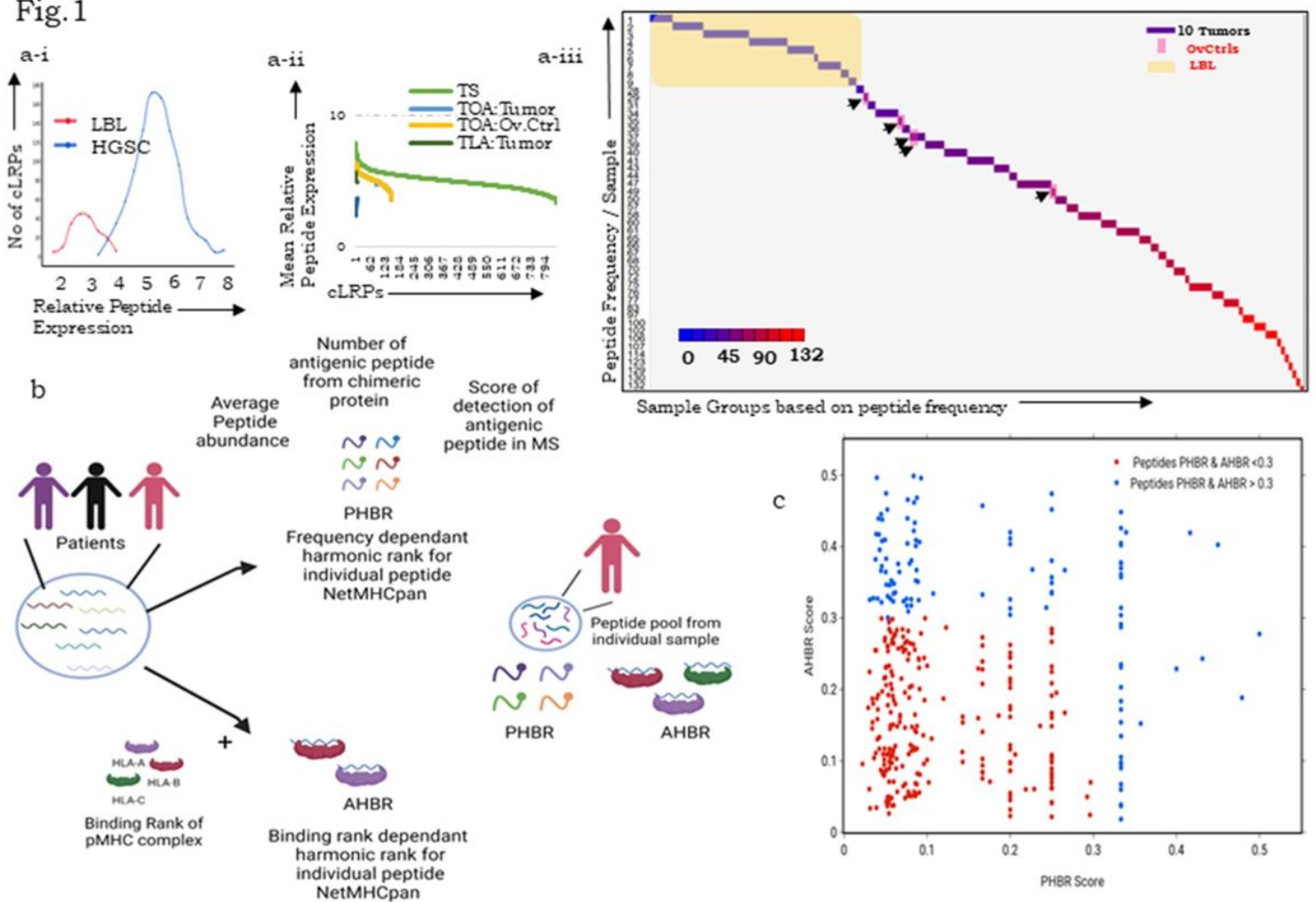


Figure 1

Identification and characterization of chimeric longest read-derived peptides (cLRPs) in OvCa. a-i. Distribution of relative peptide expression in high-grade serous ovarian tumor (HGSC) and lymphoblastoid (LBL) mass spectral data; a-ii. Relative peptide expression of cLRPs including 843 tumor specific (TS), 149 tumor- ovarian control associated (TOA), 4 tumor-LBL associated (TLA); a-iii. cLRP

frequency per sample (range 1-132 represented as 48 groups on Y-axis), lymphoblastoid (LBL, yellow highlight) and ovarian control (OvCtrl, pink highlight; arrow) associated peptides are expressed at lower frequencies than those in ovarian tumors (squares, each square representing 10 tumors), blue to red color scale indicates peptide frequency; b. Schematic indicating determination of Patient Harmonic Mean Best Rank (PHBR) and Allele Harmonic Binding Rank (AHBR); c. Scatter plot of 369 peptides with PHBR & AHBR <0.3 (red; 248 high-confidence peptides) and others with PHBR & AHBR > 0.3 (blue)

Fig.2

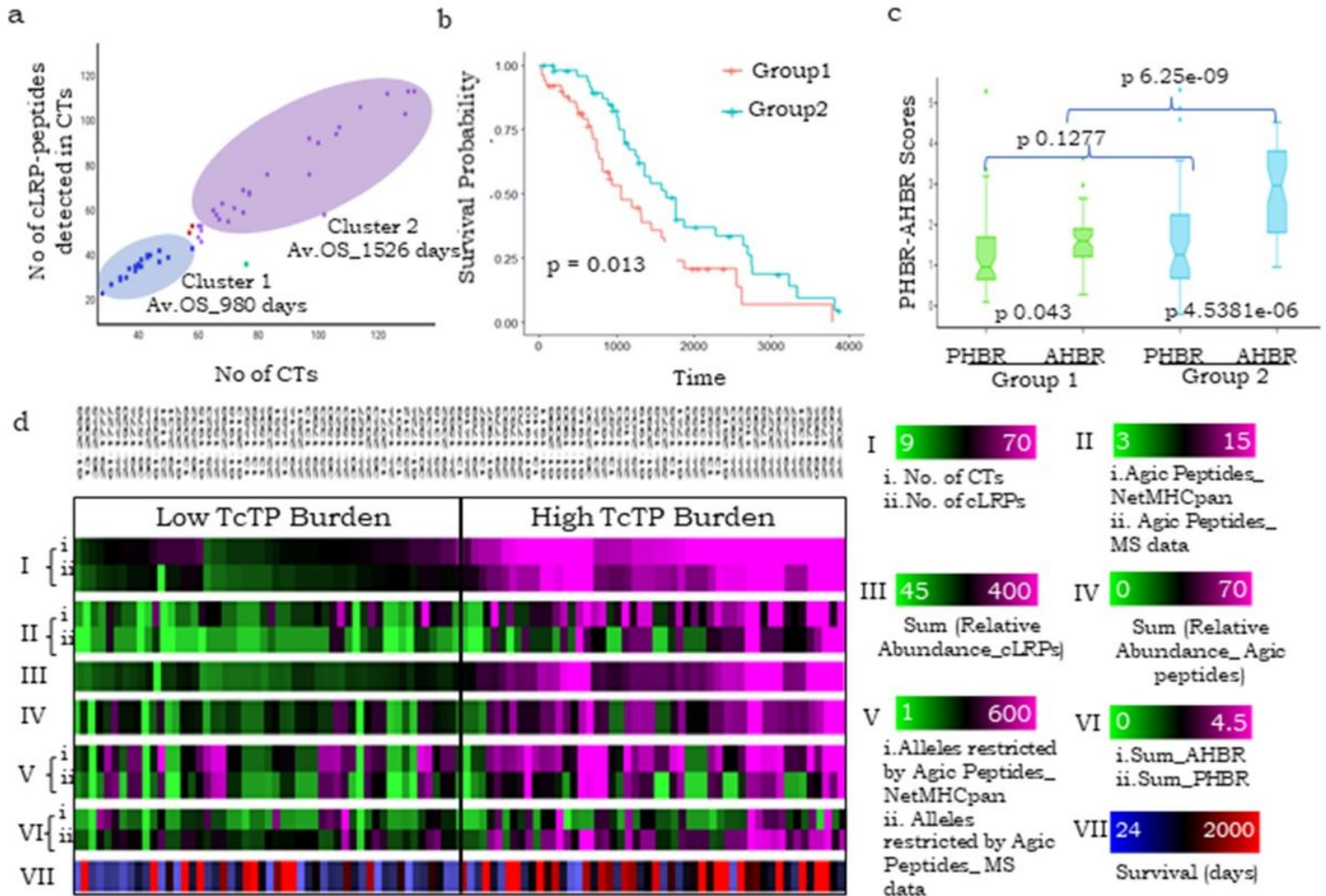


Figure 2

Tumor associated Chimeric Transcript-Protein (TcTP) burden may define allele restriction and patient prognosis in a personalized manner. a. Scatter plot representation of CT-cLRP distribution in tumors that clearly demarcates 2 clusters distinctly associated with overall survival (OS); b. KM survival plot of TcTP burden-based patient groups wherein Group 2 (higher TcTP burden) has a significant survival advantage over Group 1 (lower TcTP burden); c. Box notch plot of comparative AHBR-PHBR scores (ANOVA) within and between Group 1 and Group 2 tumors. d. Heatmap representing the differential features of the 2 patient groups including - I: number of CTs (i) and cLRPs (ii), II: number of antigenic peptides predicted in NetMHCpan (i) or detected in MS (ii), III: Sum of relative peptide abundance of all cLRPs detected in MS, V: Alleles restricted by Agic Peptides\_NetMHCpan (i) and Alleles restricted by Agic Peptides\_MS data (ii), VI: Sum\_AHBR (i) and Sum\_PHBR (ii), VII: Survival (days) data.

IV:Sum of relative peptide abundance of antigenic peptides detected in MS, V:alleles restricted by antigenic peptides predicted in NetMHCpan (i) or detected in MS (ii), VI:summation of PHBR (i) and AHBR (ii) scores of antigenic peptides, VII: Overall survival of patients; all values were mapped as per the scale bars

Fig 3

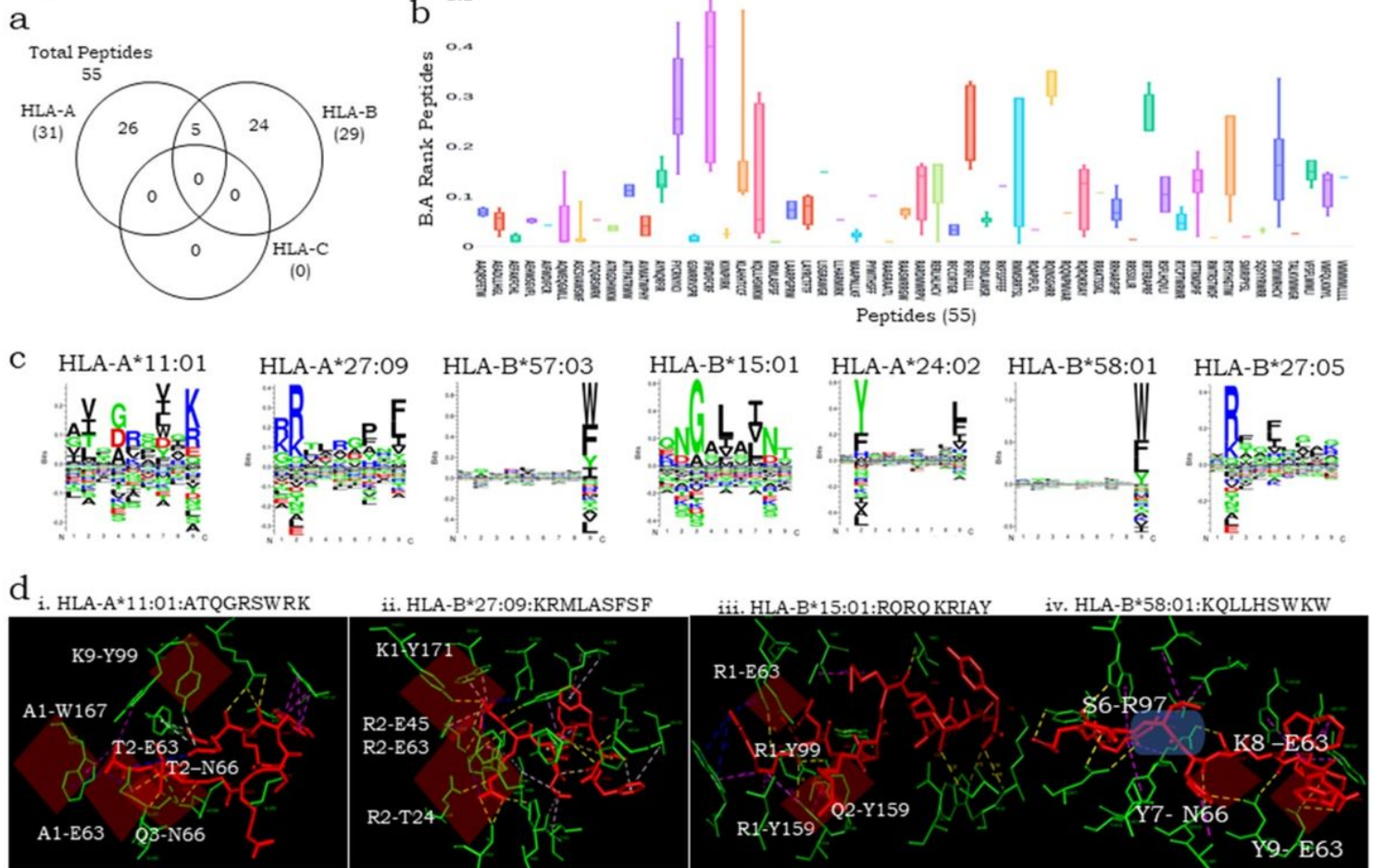


Figure 3

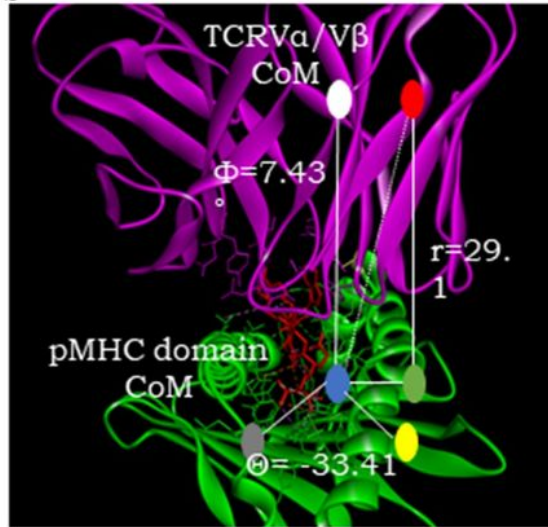
a. Haplotype-based allele restriction (NetMHCstabpan) identified 55 high confidence antigenic peptides; b. Binding Affinity (BA) Rank distribution of these 55 peptides; c. Gibbs Cluster motif generated for 7 MHC molecules HLA-A\*11:01; HLA-A\*27:09; HLA-B\*57:03; HLA-B\*15:01; HLA-A\*24:02; HLA-B\*58:01; HLA-B\*27:05 predicting positional significance of specific amino acid residues based on reported p:MHC structures; d. Predicted p:MHC interactions modelled in Discovery studio where peptide residues (red) interact with MHC residues (green) through polar (yellow), electrostatic (blue) and hydrophobic (pink) bonds, interactions are highlighted in a red cloud and salt bridge in a blue cloud, some of these interactions were also indicated in models generated in PyMOL (Table S6).

Fig.4

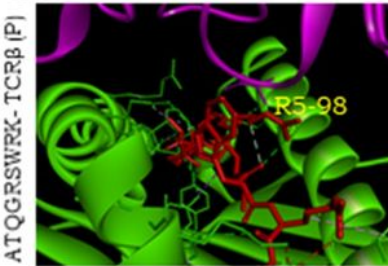
a-i



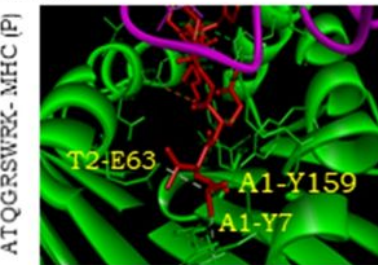
b



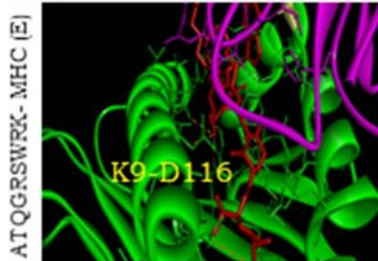
a-ii



a-iii



a-iv



c

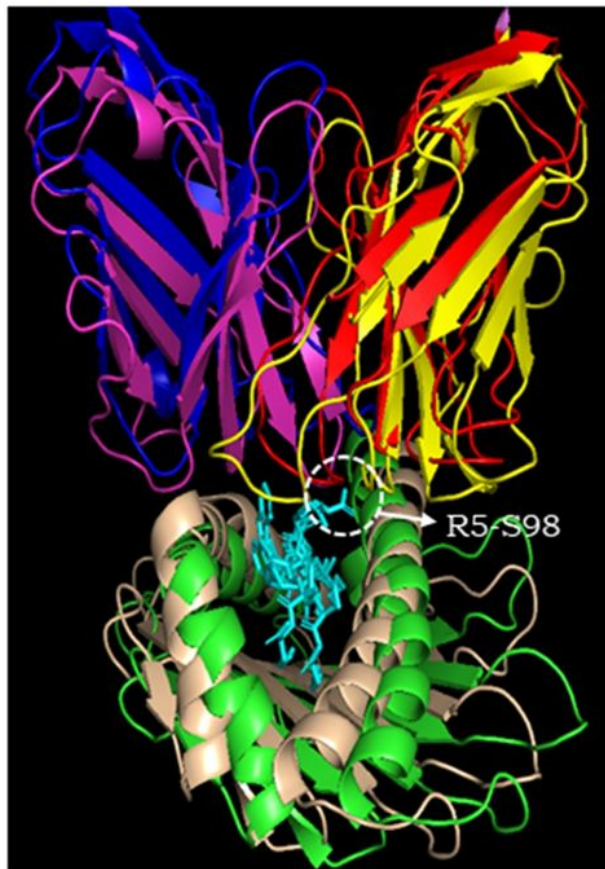


Figure 4

Molecular modeling of ATQGRSWRK:HLA-A\*11:01: TRAV21\*01/J50\*01-TRBV6.6\*01/J2.3\*01 complex (peptide-red, MHC-green, TCR-pink, polar and electrostatic interactions - green and orange bond respectively) a. Comparison of interactions with the reference models, i. 3 similar polar p:MHC interactions (A1-159, A1-Y7, T2-E63) as in RP:MHC, ii. R5-S98 polar interaction similar to RP-TCR; iii. *De novo* K9-D116 electrostatic interaction; b. Geometric parameters in the cLR-p:MHC:TCR complex where

$\Phi=7.43^\circ$  (angle between TCR:CoM and p:MHC:CoM vector),  $r=29.1$  (vector connecting TCR:CoM and p:MHC:CoM) and  $\Theta=-33.41$  (x-axis angle of projection of TCR:CoM–MHC:CoM vector); c. Comparative modeling indicating the steric hinderance for R5-S98 interactions observed by superimposing ATQGRSWRK (Cyan):HLA-A\*11:01 with the 2 reported TCRs viz. TRAV21\*01/J50\*01-TRBV6.6\*01/J2.3\*01 ( $\alpha$  chain in blue,  $\beta$  chain in red) and TRAV35\*01/J49\*01-TRBV11-2\*01/J1-2\*01 ( $\alpha$  chain in pink,  $\beta$  chain in yellow; Supplementary Figures 4 Videos 1,2).

Fig.5

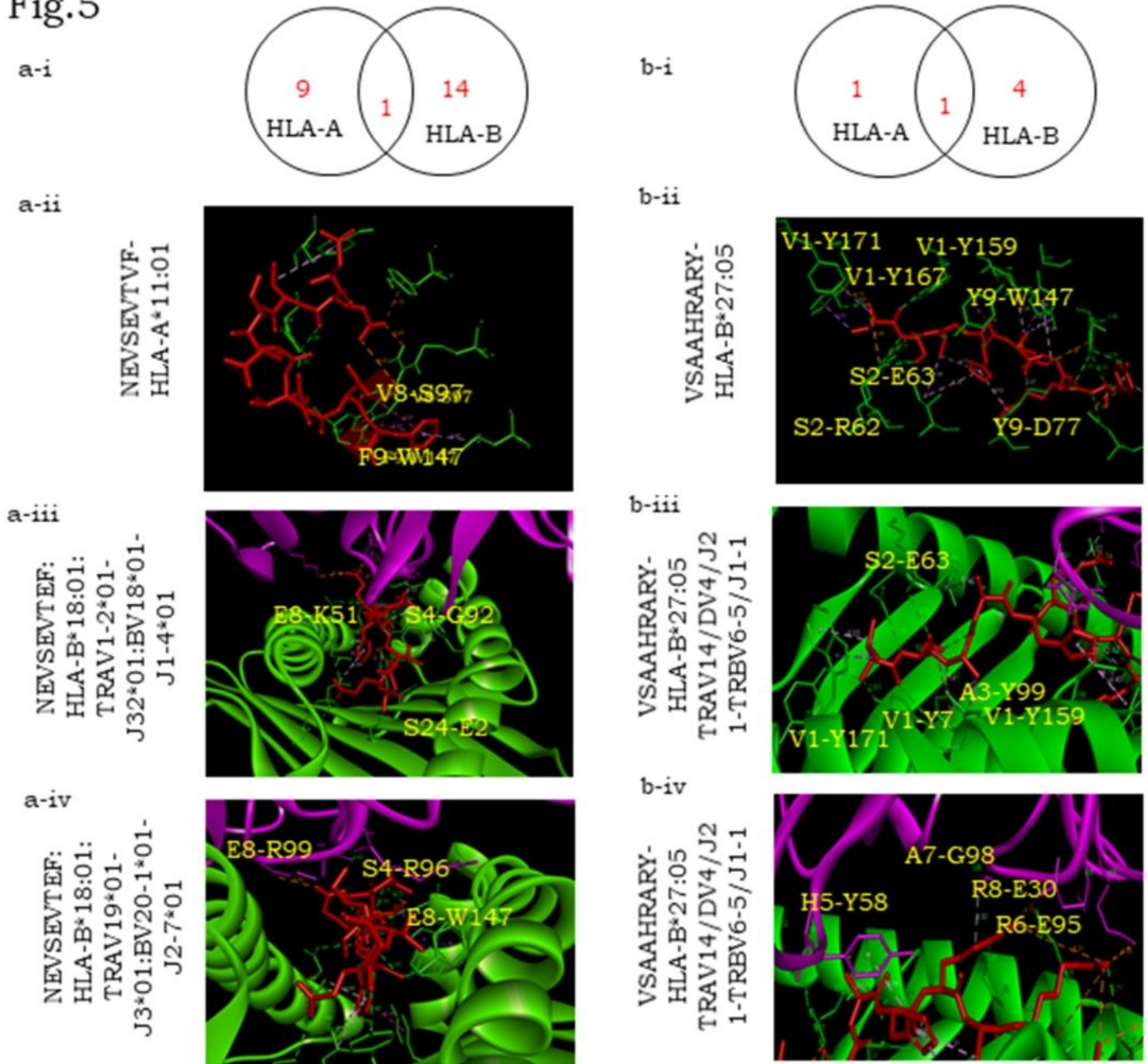


Figure 5

a-i. Venn-diagram representing HLA distribution analyses (NetMHCstabpan 1.0 to predict high stability-affinity peptides) of known immunizing mutated peptides in melanoma; a-ii. Molecular modeling of NEVSEVTVF-HLA-A\*11:01 complex (peptide-red, MHC-green) indicating two significant similar interactions; a-iii. Molecular modeling of NEVSEVTEF: HLA-B\*18:01: TRAV1-2\*01-J32\*01:BV18\*01-J1-4\*01 (peptide-red, MHC-green, TCR-pink) indicating one single interaction each of peptide with MHC (polar:E2-S24), TCR- $\alpha$  (polar:S4-G92), TCR- $\beta$  (electrostatic:E8-K51); a-iv. Molecular modeling of NEVSEVTEF: HLA-B\*18:01: TRAV19\*01-J3\*01:BV20-1\*01-J2-7\*01 (peptide-red, MHC-green, TCR-pink) indicating one single interaction each of peptide with MHC (polar:E8-W147), TCR- $\alpha$  (polar:S4-R96), TCR- $\beta$  (electrostatic:E8-R99); b-i. Venn-diagram representing HLA distribution analyses (NetMHCstabpan 1.0 to predict high stability-affinity peptides) of known immunizing mutated peptides in glioblastoma; b-ii. Representative VSAAHRARY-HLA-B\*27:05 complex where peptide (red) interacts with MHC (green) through six similar polar (V1-Y171, V1-Y159, S2-E63, S2-R62, Y9-D77, Y9-W147) and single hydrophobic (V1-W167) bonds; b-iii. Molecular modeling of complex VSAAHRARY-HLA-B\*27:05 TRAV14/DV4/J21-TRBV6-5/J1-1 (peptide-red, MHC-green, TCR-pink) indicating peptide interactions with MHC (5 similar polar:V1-Y171, V1-Y7, V1-Y159, S2-E63, A3-Y99), TCR- $\alpha$  (2 electrostatic:R6-E95, R8-E30) and TCR- $\beta$  (2 polar: A7-G98, TCR- $\alpha$  H5-Y52); b-iv. Molecular modeling of VSAAHRARY-HLA-B\*27:05 TRAV14/DV4/J21-TRBV6-5\*01/J1-1\*01 (peptide-red, TCR-pink) where peptide interacts with TCR- $\alpha$  (2 electrostatic: R6-E95, R8-E30) and TCR- $\beta$  (2 polar: A7-G98, TCR- $\alpha$  H5-Y52)

## Supplementary Files

This is a list of supplementary files associated with this preprint. Click to download.

- [SupplementaryInformation1SupplementaryMethods.pdf](#)
- [SupplementaryInformation2SupplementaryFigures.pdf](#)
- [SupplementaryInformation3SupplementaryTables112.rar](#)
- [SupplementaryInformation4SupplementaryVideos.rar](#)
- [GraphicalAbstract.tif](#)